Characterization of rate-dependent shear behavior of Zr-based bulk metallic glass using shear-punch testing

L F Liu, L H Dai,[a] and Y L Bai
State Key Laboratory of Nonlinear Mechanics (LNM), Institute of Mechanics, Chinese Academy of Science, Beijing 100080, People's Republic of China

B C Wei
National Laboratory of Microgravity, Institute of Mechanics, Chinese Academy of Science, Beijing 100080, People's Republic of China

J Eckert[b]
Department of Materials and Geo Sciences, Physical Metallurgy Division, Darmstadt University of Technology, D-64287 Darmstadt, Germany

(Received 13 May 2005; accepted 23 September 2005)

In this study, the rate-dependent mechanical behavior of a $Zr_{41.2}Ti_{13.8}Cu_{12.5}Ni_{10}Be_{22.5}$ bulk metallic glass was studied using quasi-static and dynamic shear-punch testing at room temperature. The results demonstrate that the shear strength of this alloy is insensitive to the applied strain rate. However, the formation of shear bands and the serrated flow exhibits a significant strain rate effect. The shear banding-induced fracture patterns and the fracture-melting phenomenon were analyzed based on the free volume theory and the energy transfer model.

I. INTRODUCTION

Bulk metallic glasses (BMGs) have attracted large interest due to their unique physical, mechanical, and chemical properties.[1–5] However, BMGs loaded under unconstrained conditions usually fail catastrophically with little global plasticity.[6] This deformation behavior has limited the application of BMGs as engineering material so far. At low temperatures (e.g., room temperature), plastic deformation of BMGs is usually localized into thin shear bands.[7–9] Many macroscopic mechanical properties (e.g., plasticity and ductility) are thus controlled by the individual and collective behavior of the shear bands. Furthermore, the behavior of shear bands is significantly affected by loading conditions and loading rates. Up to now, most available experimental studies on BMGs were conducted under uniaxial compression, tension, and indentation loadings. Different from compression, tension, or indentation loading modes, shear-punch testing (SPT) was performed to identify the mechanical properties of BMGs in the present work. It has been demonstrated that tensile strength data can be directly related to effective shear strength data obtained from SPT on thin specimens for a variety of materials. Thus, SPT can be successfully used to evaluate the mechanical properties of materials.[10,11] To the authors' knowledge, no data are currently available on shear-punch testing of BMGs. In view of the aforementioned observations, the mechanical properties of $Zr_{41.2}Ti_{13.8}Cu_{12.5}Ni_{10}Be_{22.5}$ bulk metallic glass under quasi-static and dynamic loading were investigated using the SPT technique. By controlling the applied load, the shear band patterns before fracture and the fracture morphologies at different applied loading rates were investigated.

II. EXPERIMENTAL

A. Sample preparation

$Zr_{41.2}Ti_{13.8}Cu_{12.5}Ni_{10}Be_{22.5}$ bulk metallic glass was produced by arc melting the pure elements (99.99%) together under a purified Ar atmosphere to obtain ingots of the desired composition. Each ingot was then re-melted four times to ensure a homogeneous composition. From these ingots, metallic glass plates with 100 mm length, 20 mm width, and 2 mm thickness were prepared by suction casting the molten alloy into a copper mold. The obtained metallic glass plates were confirmed to be noncrystalline by conventional x-ray diffraction (Siemens D5000). The specimens were machined into disks 10 mm in diameter and 1.5 mm thick. The samples were then fine polished in preparation for testing. For each condition, 6–10 specimens were tested.

[a]Address all correspondence to this author
e-mail: lhdai@lnm.imech.ac.cn
[b]This author was an editor of this journal during the review and decision stage. For the *JMR* policy on review and publication of manuscripts authored by editors, please refer to http://www.mrs.org/publications/jmr/policy.html
DOI: 10.1557/JMR.2006.0006

B. Mechanical testing

Shear-punch testing was performed using a specially designed fixture [Fig. 1(a)] in an MTS 810 material testing system and a split-Hopkinson pressure bar (SHPB) apparatus, respectively. The quasi-static tests were conducted with a MTS 810 material testing system at a cross-head speed of 0.06 mm/min with a 6-mm-diameter punch. The load applied was continuously monitored as a function of punch head displacement. To investigate the evolution of shear bands in the specimens, the applied loads were unloaded at different values. As illustrated in Fig. 1(b), the shear stress was calculated using the following relation

$$\tau = \frac{P}{2\pi r_{avg} H} \quad , \tag{1}$$

where $r_{avg} = (r_{punch} + r_{die})/2$, P is the applied load, and

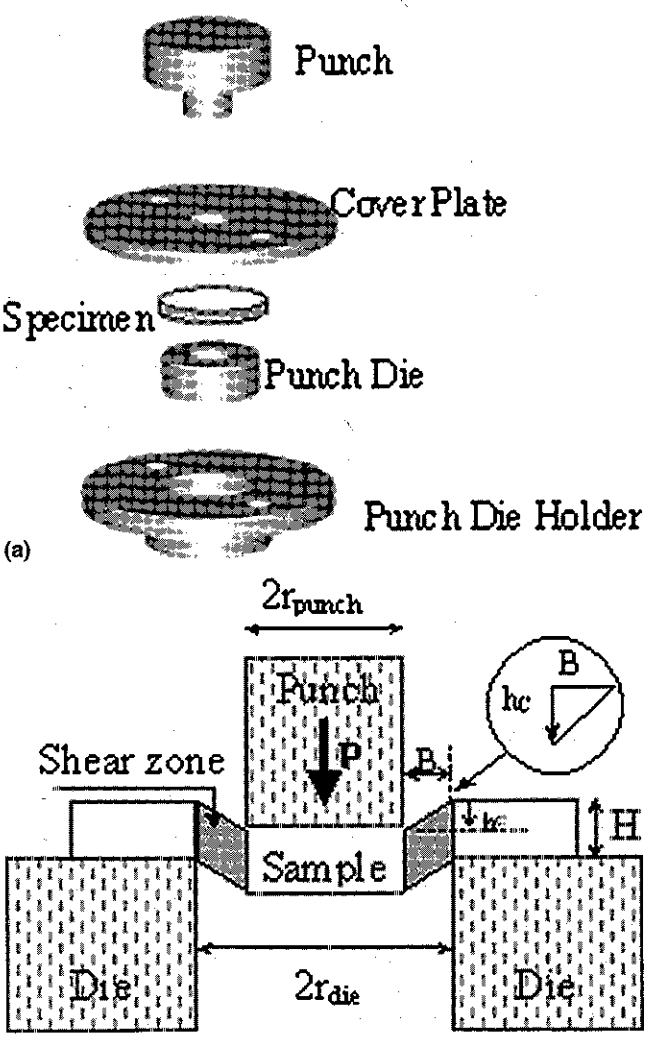

FIG. 1. (a) Shear-punch test setup and (b) schematic illustration of shear-punch test

H is the specimen thickness. The true multiaxial, nonuniform stress state in the annular shear zone is relatively uniform shear combined with a compressive stress of smaller magnitude. The net effect of these multiaxial, nonuniform stresses for shear-punch tests, relative to a pure shear stress state, appears to be mostly a modification of the correlation constants connecting shear-punch stresses with tensile test stresses [11]. Since these constants must be established experimentally, it is reasonable to adopt Eq. (1) as an appropriate operational definition of the stress for shear punch tests.

To obtain the accurate displacement of the punch, the measuring method of crack opening displacement (COD) was adopted. Moreover, there is an influence of the punch compliance because a portion of the punch is below the punch-COD coupling. The resultant punch displacement (h_r) was obtained by subtracting the elastic compression (δ) of the punch from the punch displacement measured by the COD (h_C),

$$h_r = h_C - \delta = h_C - L\frac{P}{E\pi r^2} \tag{2}$$

E is the Young's modulus of the punch material, P is the load, and L is the length of the punch that is below the COD coupling. Under quasi-static loading, the shear strain and the shear strain rate were normalized by the die-punch clearance B, and they were defined as shear strain $\gamma = (h_r/2B)$; and shear strain rate $\dot{\gamma} = (\dot{h}_r/2B)$.

The dynamic tests were conducted with a split-Hopkinson pressure bar (SHPB) apparatus at impact speeds of 16, 20, and 22 m/s with a 6-mm-diameter punch. The evolution of shear bands was achieved through modifying the impact speed. The normalized strain rate, normalized strain, and shear stress can be calculated according to the incident wave $\epsilon_i(t)$, the reflected wave $\epsilon_r(t)$, measured by the gauges on the input bar, and the transmitted wave $\epsilon_t(t)$, measured by the gages on the output bar as follows[12]

$$\dot{\gamma} = -\frac{C_b}{B}\epsilon_r(t) \quad , \tag{3}$$

$$\gamma = -\frac{C_b}{B}\int_0^t \epsilon_r(t)\mathrm{d}t \quad , \tag{4}$$

$$\tau = \frac{A_b E_b}{2\pi r_{avg} H}\epsilon_r(t) \quad , \tag{5}$$

where A_b, E_b, and C_b are the cross-section area, elastic modulus, and elastic wave velocity of the pressure bar, respectively. Under dynamic loading, the shear strain and the shear strain rate were also normalized by the die-punch clearance B.

C. Observation of shear bands and fracture morphology

To understand the shear band behavior and the shear fracture mechanisms of the material, the surfaces before fracture and the fracture surface morphologies of deformed samples were carefully examined by scanning electron microscopy (SEM; FEI-Sirion NC microscope).

III. EXPERIMENTAL RESULTS

A. Mechanical behavior

The shear stress versus normalized shear strain curves obtained under both quasi-static and dynamic loading of the $Zr_{41.2}Ti_{13.8}Cu_{12.5}Ni_{10}Be_{22.5}$ bulk metallic glass are shown in Fig. 2. The normalized shear strain rates are 5.6×10^{-4} s^{-1} and 6.0×10^{3} s^{-1}, respectively. It can be seen from Fig. 2 that, for both typical strain rates, the material exhibits a "quasi-brittle" behavior and little macroscopic plastic flow (about 0.1%). After the peak stress, the stress dropped immediately. The peak shear stress or shear strength is about 1100 MPa for the quasi-static strain rate and 1140 MPa for the dynamic strain rate. This means that under shear punch testing, the shear strength of this material is relatively insensitive to the strain rate. The present result is consistent with the experimental observation of Lu et al. for compression testing of this alloy [13]. At quasi-static loading conditions, the flow is noted to be serrated. This is similar to that what has been previously observed for other loading modes [14–19]. Also, serrated flow has been proposed to be associated with the emission of localized shear bands [14]. It is of interest to note that the amplitude of the serrated flow decreases with increasing strain rate. This is similar to previous reports on BMGs under different loading conditions [14–19]. Actually, the flow serration gradually diminishes at the strain rate of 6.0×10^{3} s^{-1}.

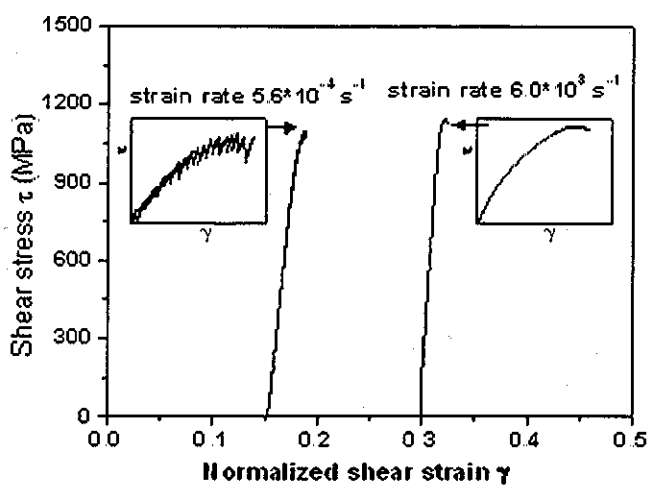

FIG. 2. Shear stress–strain curves of the $Zr_{41.2}Ti_{13.8}Cu_{12.5}Ni_{10}Be_{22.5}$ bulk metallic glass at different strain rates.

B. Shear band behavior and fracture morphology

The SEM micrographs of the punch-deformed surfaces subjected to normalized strain rates of 5.6×10^{-4} s^{-1} and 6.0×10^{3} s^{-1} are presented in Figs. 3(a) and 3(b), respectively. The stress corresponding to these photographs is about 1000 MPa. It is readily found that, under both quasi-static and dynamic strain rates, a circular deformed region on the sample surface can be observed. The result demonstrates that the designed fixture and specimen can effectively ensure the deformation under the prescribed shear-punch condition.

The micrographs in Figs. 4(a) and 4(b) depict the local morphology around the circular deformation region under quasi-static and dynamic strain rates. Figure 4(a) displays the local deformation pattern under quasi-static strain rate. From the micrograph, a few shear bands can be clearly observed in the circular deformation region.

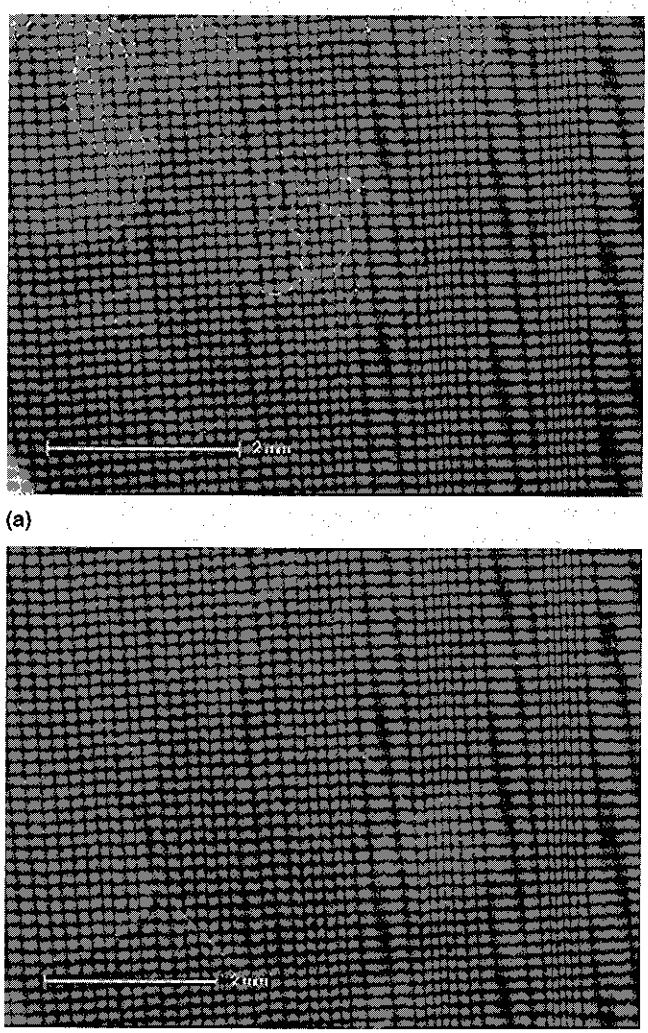

FIG. 3. SEM micrographs of the overall appearance of the punch-deformed surfaces under normalized strain rates of (a) 5.6×10^{-4} s^{-1} and (b) 6.0×10^{3} s^{-1}.

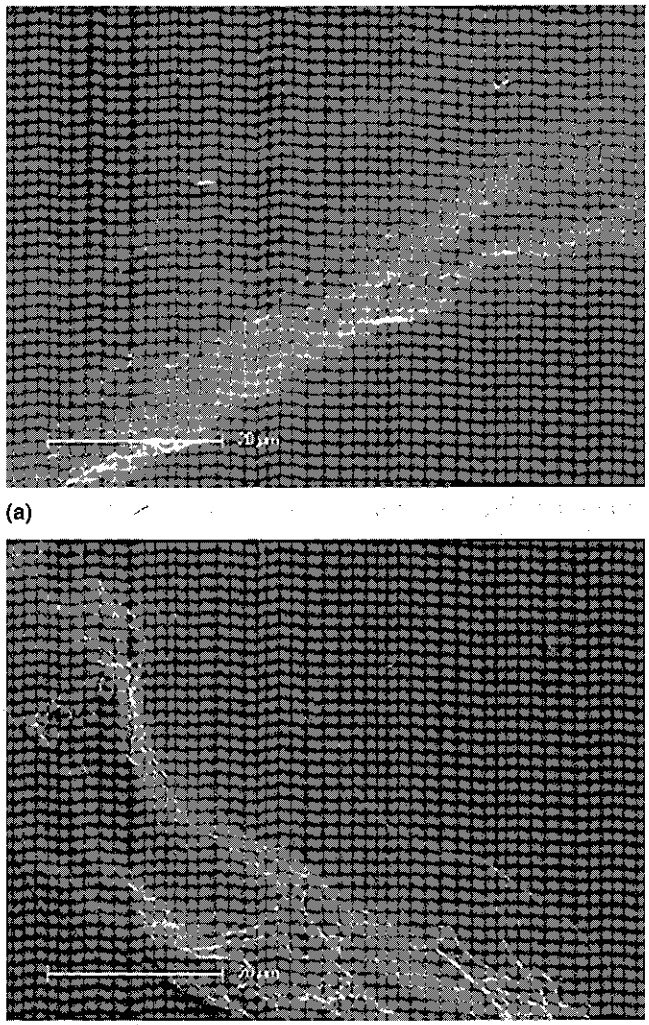

(a)

(b)

FIG. 4 SEM micrographs of the deformation pattern obtained at higher magnification under normalized strain rates of: (a) 5.6×10^{-4} s^{-1} and (b) 6.0×10^{3} s^{-1}

These shear bands are distributed along the circular deformation region. Compared with the quasi-static loading case, the density of shear bands formed at dynamic strain rate is relatively high. This observation is consistent with the findings of Mukai et al.[15] for dynamic tensile testing, Schuh et al.,[16] Jiang et al.,[17] and Dai et al.[18] for nanoindentation, as well as with the results of Liu et al.[19] for compression testing. The difference in the density of shear bands indicates that the formation of shear bands is significantly dependent on the strain rate; i.e., the density of shear bands at the dynamic strain rate is higher than that under quasi-static strain rate conditions. The aforementioned stress–strain curves demonstrate that the amplitude of the serrated flow decreases with increasing strain rate. The facts that the density of shear bands increases and the serrated flow diminishes with increasing loading rate demonstrate that the serrated flow depends on the individual behavior of single shear bands, and the collective behavior of numerous shear bands will suppress the serrated flow.

The typical fracture morphology of the $Zr_{41.2}Ti_{13.8}Cu_{12.5}Ni_{10}Be_{22.5}$ BMG under quasi-static strain rate is shown in Fig. 5(a). The shear-punch fracture surface can be divided into two characteristic zones along the shear loading direction, which are the fracture initiation zone (I) and the fast facture zone (II). In the slip zone (I), except for some strips and traces of microcracks, as shown in the magnified area displayed in Fig. 5(b), no melting phenomenon can be observed. With accelerated propagation of the fracture cracks, the fracture turns into the fast fracture zone (II), where vein patterns and melted droplets can be readily observed. It is very interesting to see that the fracture morphology is changed in the middle of zone (II), as shown in the high magnification micrograph Fig. 5(c) of this zone. The melting region in the second part is much larger than that in the first part along the crack propagating direction.

The typical fracture morphology of the $Zr_{41.2}Ti_{13.8}Cu_{12.5}Ni_{10}Be_{22.5}$ BMG under dynamic strain rate is shown in Fig. 6(a). The shear-punch fracture surface can also be divided into two characteristic zones along the shear loading direction: the fracture initiation zone (I) and the fast facture zone (II). However, compared with the quasi-static case, the most obvious difference is that there was not any obvious changes of fracture morphology could be observed in zone (II). Simultaneously, the area of the melted regions is larger than under quasi-static loading. These observations demonstrate that the sample fractured rapidly with little changes. Figures 6(b)–6(d) show high magnification micrographs corresponding to the regions shown in Figs. 5(b)–5(d). Figures 6(b)–6(d) also demonstrate that the fracture under dynamic strain rate is different from that under quasi-static strain rate. The fracture morphologies (Figs. 5 and 6) of the $Zr_{41.2}Ti_{13.8}Cu_{12.5}Ni_{10}Be_{22.5}$ BMG demonstrate that, under shear-punch loading, the fracture process depends on the loading rate. The fracture morphologies under quasi-static loading are obviously different from that under dynamic loading.

IV. DISCUSSION

The above experimental observations reveal that the serrated flow, the density of shear bands, and the fracture morphology are strongly affected by the strain rate or loading rate, although the shear strength for this alloy is relatively insensitive to the stain rate. Serrated flow of BMGs is most commonly observed under uniaxial compression[14,19] and nanoindentation.[16–18] Furthermore, these serrations have been correlated with the motion of individual shear bands in the sample, where each shear

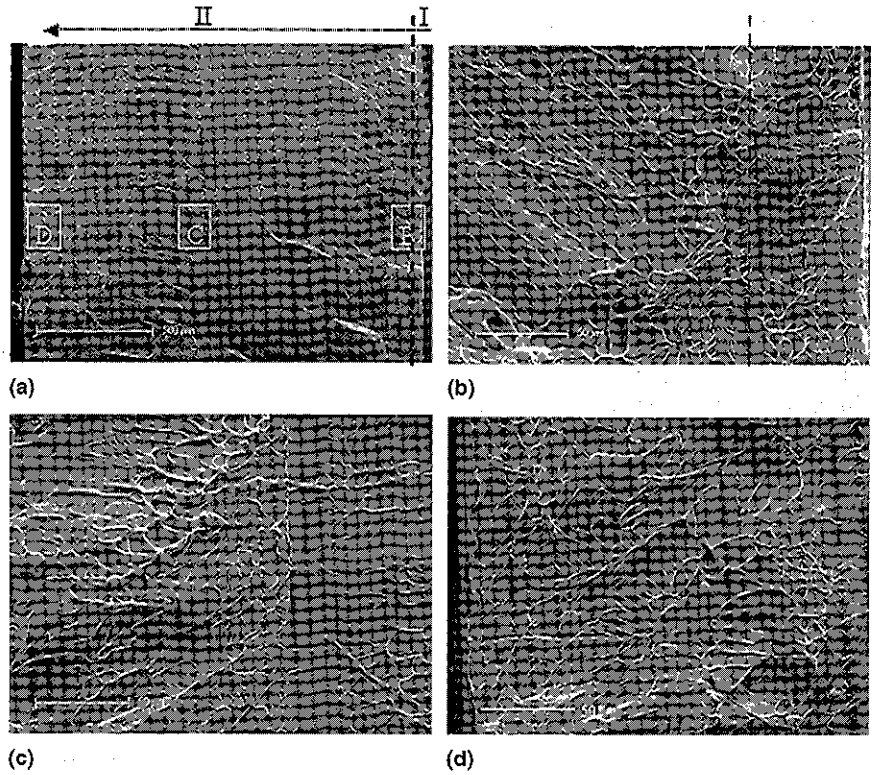

FIG. 5. Typical fracture morphology of the $Zr_{41.2}Ti_{13.8}Cu_{12.5}Ni_{10}Be_{22.5}$ bulk metallic glass deformed at 5.6×10^{-4} s^{-1}

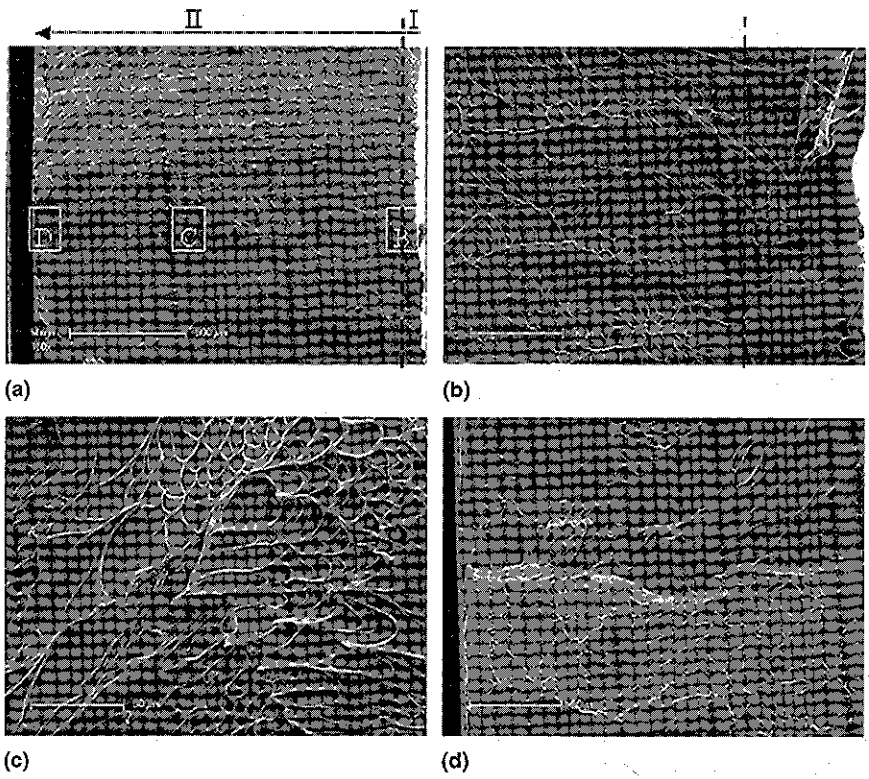

FIG. 6. Typical fracture morphology of the $Zr_{41.2}Ti_{13.8}Cu_{12.5}Ni_{10}Be_{22.5}$ bulk metallic glass deformed at 6.0×10^{3} s^{-1}

band contributes a small increment of plastic strain to the macroscopic stress–strain curve.[14] Simultaneously, the density of shear bands depends on the loading rate, suggesting that shear band nucleation and propagation are rate-dependent processes.[16] However, the mechanisms for this rate-dependent shear banding behavior are not well understood.

Physically, a rate effect such as observed in Fig. 4 is consistent with the notion that shear banding is an inherently nucleation-dominated process.[20–22] This process is not only affected by the amplitude of the imposed loads, but also affected by the externally imposed strain rates. For a low externally imposed strain rate, the very high local shear rate in a shear band can be decreased with enough time. This implies rapid unloading of the loading system and stop of plastic deformation, i.e., repeated load serrations occur with single shear band. New shear bands are nucleated again when the stress rises and approaches the necessary value. However, for a very high external strain rate, such unloading is highly suppressed,[23] the stress remaining at the high nuclea-tion value of shear bands. Thus, to accommodate the imposed high strain rate, a large number of shear bands may originate. Microscopically, the formation of a shear band in BMGs occurs first by the local free volume softening. The rate effect in this process is the formation of a shear-band embryo from a local free volume increasing and coalescence. Finally, the rate effect of the formation of shear band can be characterized by the rate effect of the net creation or evaluation of the free volume in BMGs.

According to the free volume theory,[20–22 24] the formation of shear bands in metallic glasses is mainly due to the creation and coalescence of free volume, and the creation and diffusion of free volume in metallic glasses are greatly affected by the strain rate. From Turnbull–Cohen's free volume theory,[24 25] Spaepen developed a general constitutive equation to characterize the plastic flow of metallic glasses.[20] According to this model, the shear strain rate can be written as

$$\dot{\gamma} = \frac{\dot{\tau}}{\mu} + 2f\exp\left(-\frac{\alpha}{\xi}\right)\exp\left(-\frac{\Delta G}{k_B T}\right)\sinh\left(\frac{\tau\Omega}{k_B T}\right) \quad , \tag{6}$$

where τ is the applied shear stress, $\dot{\gamma}$ is the shear strain rate, ξ is the concentration of the free volume, α is a geometrical factor of the order of unity, f is the frequency of atomic vibration, ΔG is the activation energy, Ω is the atomic volume, k_B is Boltzmann's constant, μ is the shear modulus, and T is the absolute temperature. Equation (6) shows that the concentration of the free volume ξ plays a key role in the deformation of metallic glasses. An as-prepared metallic glass is thermodynamically unstable and has a nonequilibrium amount of free volume. During deformation under a shear stress, additional free volume is continuously created by the applied shear stress and, on the other hand, annihilated by structural relaxation due to atomic rearrangements. In the flow model developed by Spaepen,[20] the free volume is created by an applied shear stress τ and annihilated by a series of atomic jumps, and the net rate of the change of the free volume concentration is

$$\frac{\partial\xi}{\partial t} = f\exp\left(-\frac{\alpha}{\xi}\right)\exp\left(-\frac{\Delta G}{K_B T}\right)\left\{\frac{2\alpha K_B I}{S\xi V^*}\left[\cosh\left(\frac{\tau\Omega}{2K_B T}\right) - 1\right] - \frac{1}{n_D}\right\} \quad , \tag{7}$$

where n_D is the number of atomic jumps needed to annihilate a free volume equal to V^*, $S = 2(1 + \nu)/3(1 - \nu)\,\mu$, and ν is Poisson's ratio. By numerically solving Eqs. (6) and (7), the shear stress–strain curves and the evolution of the free volume concentration can be obtained. In the calculation, we take $\alpha = 0.15$, $f = 1 \times 10^{13}\ s^{-1}$, $\Delta G = 1 \times 10^{-19}$ J, $\Omega = 26.1 \times 10^{-30}\ m^3$, $k_B = 13.8 \times 10^{-24}$ J/K, $\mu = 35.3$ GPa, $V^* = 0.8\,\Omega$, $\nu = 0.36$, and $T = 300$ K. The shear stress and the concentration of free volume are assumed to be zero and 0.008, respectively in the initial configuration. The dimensionless shear stress and the free volume concentration varying with shear strain for a typical strain rate of $\dot{\gamma} = 1.0 \times 10^{-2}\ s^{-1}$ are shown in Fig. 7. The effect of shear strain rate on the steady value of the dimensionless free volume concentration is presented in Fig. 8. Obviously, the dimensionless free volume concentration is sensitive to the shear strain rate; i.e., the dimensionless free volume concentration increases with increasing shear strain rate.

It can be seen from Fig. 7 that for those relatively low stresses, the free volume annihilation rate exactly balances the stress-driven creation rate. As a result, the total concentration of free volume remains constant. With the

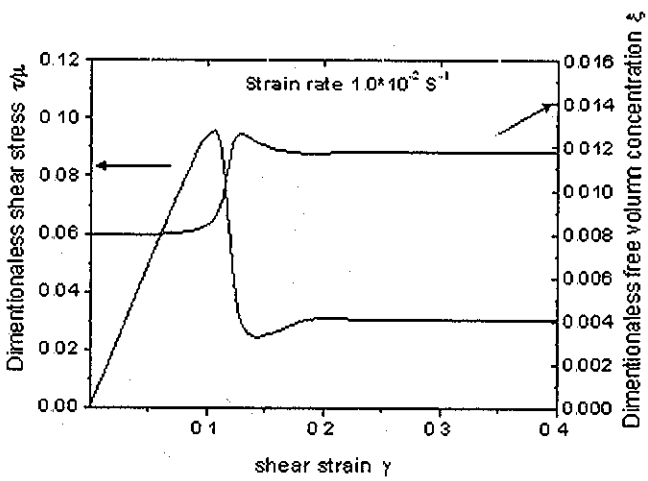

FIG. 7. Dimensionless shear stress and free volume concentration as a function of shear strain.

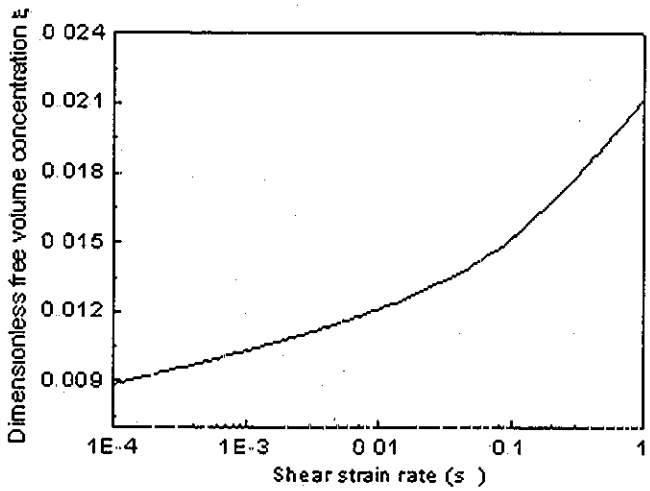

FIG 8 Free volume concentration as a function of shear strain rate

applied load increasing further, the creation rate exceeds the annihilation rate, which results in a distinct drop in shear stress Eventually, the annihilation rate again balances the creation rate, and the steady state value of the concentration of free volume is reached It is noted from Fig 7 that the steady value of the concentration of free volume is larger than the initial value More importantly, it can be found from Fig 7 that the total concentration of free volume in metallic glasses is significantly affected by the strain rate: the higher the strain rate, the higher the concentration of free volume As mentioned above, the coalescence of free volume is a key reason for the formation of shear bands in BMGs Therefore, a relatively higher concentration of free volume will promote the initiation of shear bands in BMGs The experimental observation that the number of shear bands initiated at dynamic strain rates is larger than that at quasi-static strain rates can be mainly attributed to this reason

However, this does not mean that the local heating induced by the dissipated work of deformation does not play a role in the formation of shear bands in BMGs for any cases At high strain rates ($\gamma \geq 10^2\ s^{-1}$), the local heating within the shear localization zone may exert an influence on the shear band formation in BMGs Hence, further studies are still needed to be performed to discern this effect at high strain rates

Once shear bands are initiated in the alloy, one dominant shear band will propagate fast and fracture occurs immediately Figures 5 and 6 show the fracture morphologies at the quasi-static and dynamic strain rates, respectively Since the fracture morphology is created by shear band propagation, a close-up examination on the characteristic features of the fracture morphology can help us understand the shear band propagation behavior and the fracture mechanism It can be seen from Fig 5 and Fig 6 that melted regions can be observed under both quasi-static and dynamic shear loading The melting phenomenon demonstrates that the temperature of the shear region has exceeded the melting temperature of the tested material The local increase in temperature can be estimated by considering the conversion of the stored elastic strain energy into adiabatic heating of a localized region at the moment of shear fracture From Fig 1, the total elastic strain energy (E_e) can be estimated by the following equation

$$E_e = \tau_f \gamma_e 2\pi\, r_{avg} H B \quad , \tag{8}$$

where τ_f and γ_e are the fracture strength and the elastic strain of the material $r_{avg} = (r_{punch} + r_{die})/2$, H is the specimen thickness, and B is the die-punch clearance in the deformation region

Since all plastic deformation is localized in the shear deformation bands, it is reasonable to assume that the elastic strain energy is dissipated in the shear band region at fracture,[26] resulting in adiabatic heating in this region The term E_e can thus be correlated with the temperature increase in the shear band region by the following equation

$$K E_e = 2\pi\, r_{avg} H W_S \rho C_p \Delta T \quad , \tag{9}$$

where W_s is the thickness of the shear band, ρ is the mass density of the alloy, C_p is the specific heat, and K (at 0.95) is the work-heat transformation coefficient For the present material, $\rho = 6000\ kg/m^3$ and $C_p = 450\ J/(kg\ K)$ [27] According to the experimental results, $\tau = 1100$ MPa, $\gamma_c = 0.02$, $B = 0.2$ mm, and $W_s \approx 0.8\ \mu m$ Inserting these values into Eq (9), the possible temperature rise in the shear bands is about 1830 K The melting temperature of the tested material is 936 K Obviously, the adiabatic shear-induced temperature rise in the shear bands at fracture exceeds the melting temperature of the material This is why numerous liquid droplets and melted belts can be clearly observed on the fracture surfaces A similar high adiabatic temperature rise in BMGs was observed by the other investigators [26,28,29] For example, by using a high-speed infrared technique, Bruck et al.[28] detected a temperature increase of more than 500 K in the sample surface zone of $Zr_{41.2}Ti_{13.8}Cu_{12.5}Ni_{10}Be_{22.5}$ glassy specimens tested under dynamic compressive loading at room temperature Liu et al.[26] reported a temperature rise by 900 K-inside the shear bands for a Zr–Al–Cu–Ni bulk metallic glass subjected to tensile loading For our samples, it is noted that the relatively rough fracture surface and the melted droplets on the fracture surface at dynamic strain rates means that the dissipated energy during dynamic shearing is larger than in the quasi-static case This is perhaps the reason that the measured fracture toughness of this alloy dramatically increases at high strain rates [30]

V. CONCLUSIONS

The strain rate-dependent mechanical properties of a $Zr_{41.2}Ti_{13.8}Cu_{12.5}Ni_{10}Be_{22.5}$ bulk metallic glass were investigated using shear-punch testing. The results demonstrate that the formation behavior of shear bands and the fracture of this material are strongly affected by the strain rate. The density of shear bands increases and the serrated flow diminishes with increasing strain rate. The serrated flow can be easily distinguished under quasi-static strain rate while it diminishes under dynamic strain rate. The finding that the serrated flow exhibits an inverse relation to the density of shear bands reveals that the serrated flow depends on the individual behavior of single shear bands, and the collective behavior of numerous shear bands will suppress the serrated flow. Numerous liquid droplets and melted belts on the fracture surfaces demonstrate that the temperature rise at fracture might exceed the melting temperature of the material.

ACKNOWLEDGMENTS

The authors gratefully acknowledge the financial support of this work by the National Natural Science Foundation of China through Grant Nos. 10472119 and 10232040.

REFERENCES

1. H S. Chen: Glassy metals *Rep. Prog. Phys.* **43,** 353 (1980)
2. A. Inoue and T. Zhang: Al–La–Ni amorphous-alloys with a wide supercooled liquid region *Mater. Trans. JIM* **30,** 965 (1989)
3. A.L. Greer: Metallic glasses *Science* **267,** 1947 (1995).
4. W.L. Johnson: Bulk glass-forming metallic alloys: Science and technology *MRS Bull* **24,** 42 (1999).
5. J. Eckert, A. Kübler, and L. Schultz: Mechanically alloyed $Zr_{55}Al_{10}Cu_{30}Ni_5$ metallic glass composites containing nanocrystalline W particles *J. Appl. Phys* **85,** 7112 (1999)
6. Z.F. Zhang, G. He, J. Eckert, and L. Schultz: Fracture mechanisms in bulk metallic glassy materials *Phys. Rev. Lett* **91,** 045505 (2003)
7. W.H. Wang, C. Dong, and C.H. Shek: Bulk metallic glasses *Mater. Sci. Eng. R* **44,** 45 (2004)
8. C.A. Pampillo: Localized shear deformation in a glassy metal *Scripta Metall.* **6,** 915 (1972)
9. R.D. Conner, W.L. Johnson, N.E. Paton, and W.D. Nix: Shear bands and cracking of metallic glass plates in bending *J. Appl. Phys* **94,** 904 (2003)
10. G.L. Hankin, M.B. Toloczko, M.L. Hamilton, F.A. Garner, and R.G. Faulkner: Shear punch testing of 59Ni isotopically-doped model austenitic alloys after irradiation in FFTF at deferent He/dpa ratios. *J. Nucl. Mater.* **258A,** 1657 (1998)
11. G.L. Hankin, M.B. Toloczko, K.I. Johnson, M.A. Khaleel, M.L. Hamilton, F.A. Garner, R.W. Davies, and R.G. Faulkner: Improvement of post irradiation ductility of V-Ti-Cr-Si type alloys Neutron irradiated around 400C. *ASTM STP* **1366,** 1018 (2000)
12. L.H. Dai and Y.L. Bai: Transverse shear strength of unidirectional carbon fiber reinforced aluminium matrix composite under static and dynamic loadings. *J. Compos. Mater.* **32,** 246 (1998)
13. J. Lu, G. Ravichandran, and W.L. Johnson: Deformation behavior of the $Zr_{41.2}Ti_{13.8}Cu_{12.5}Ni_{20}Be_{22.5}$ bulk metallic glass over a wide range of strain-rates and temperatures. *Acta Mater.* **51,** 3429 (2003).
14. W.J. Wright, R.B. Schwarz, and W.D. Nix: Localized heating during serrated plastic flow in bulk metallic glasses. *Mater. Sci. Eng. A* **319–321,** 229 (2001)
15. T. Mukai, T.G. Nieh, Y. Kawamura, A. Inoue, and K. Higashi: Dynamic response of a $Pd_{40}Ni_{40}P_{20}$ bulk metallic glass in tension. *Scripta Mater.* **46,** 43 (2002)
16. C.A. Schuh and T.G. Nieh: A survey of instrumented indentation studies on metallic glasses. *J. Mater. Res.* **19,** 46 (2004).
17. W.H. Jiang and M. Atzmon: Rate dependence of serrated flow in a metallic glass. *J. Mater. Res.* **18,** 75 (2003)
18. L.H. Dai, L.F. Liu, M. Yan, B.C. Wei, and J. Eckert: Serrated plastic flow in a Zr-based bulk metallic glass during nanoindentation. *Chin. Phys. Lett.* **21,** 1593 (2004)
19. L.F. Liu, L.H. Dai, Y.L. Bai, B.C. Wei, and G.S. Yu: Strain rate-dependent compressive deformation behavior of Nd–based bulk metallic glass. *Intermetallics* **13,** 827 (2005)
20. F. Spaepen: A microscopic mechanism for steady state inhomogeneous flow in metallic glasses. *Acta Metall.* **25,** 407 (1977)
21. A.S. Argon: Plastic deformation in metallic glasses. *Acta Metall* **27,** 47 (1979).
22. P.S. Steif, F. Spaepen, and J.W. Hutchinson: Strain localization in amorphous metals. *Acta Metall.* **30,** 447 (1982).
23. A. Yu. Vinogradov and V.A. Khonik: Kinetics of shear banding in a bulk metallic glass monitored by acoustic emission measurements. *Philos. Mag.* **84,** 2147 (2004).
24. M.H. Cohen and D. Turnbull: Molecular transport in liquids and glasses. *J. Chem. Phys.* **31,** 1164 (1959)
25. D. Turnbull and M.H. Cohen: Free-volume model of the amorphous phases: Glass transition. *J. Chem. Phys.* **34,** 120 (1961).
26. C.T. Liu, L. Heatherly, D.S. Easton, C.A. Carmichael, J.H. Schneibel, C.H. Chen, J.L. Wright, M.H. Yoo, J.A. Horton, and A. Inoue: Test environments and mechanical properties of Zr-Base bulk amorphous alloys metall. *Mater. Trans. A* **29,** 1811 (1998)
27. T. Benameur, K. Hajlaoui, A.R. Yavari, and A. Inoue: On the characterization of plastic flow in Zr-based metallic glass through micro-indentation: An atomic force microscopy analysis. *Mater. Trans.* **43,** 2617 (2002).
28. H.A. Bruck, A.J. Rosakis, and W.L. Johnson: The dynamic compressive behavior of beryllium bearing bulk metallic glasses. *J. Mater. Res.* **11,** 503 (1996).
29. V.Z. Bengus: Solid state phenomena, in *Non-Linear Phenomena in Materials Science II,* edited by G. Martin and L. Kubin (Trans Tech Publications, Zurich, Switzerland, 1992), p. 347
30. D.M. Owen, A.J. Rosakis, and W.L. Johnson: Fracture toughness determination for a beryllium-bearing bulk metallic glass, in *Bulk Metallic Glasses,* edited by W.L. Johnson, A. Inoue, and C.T. Liu (Mater. Res. Soc. Symp. Proc. **554,** Warrendale, PA, 1999), p. 419.